2007 IEEE International Conference on
Robotics and Automation
Roma, Italy, 10-14 April 2007

Dynamic Stability of Off-Road Vehicles Considering a Longitudinal Terramechanics Model

Zvi Shiller, Moshe P. Mann, and Dror Rubinstein
Department of Mechanical Engineering-Mechatronics
The College of Judea and Samaria
shiller@yosh.ac.il

Abstract— **Dynamic stability reflects the vehicle's ability to traverse uneven terrain at high speeds. It is determined from the set of admissible speeds and tangential accelerations of the center of mass along the path, subject to the ground force and geometric path constraints. This paper presents an analytical method for computing the stability margins of a planar all-wheel drive vehicle that accounts for soil parameters. It consists of mapping the ground force constraints to constraints on the vehicle's speeds and accelerations along the path. The boundaries of the set of admissible speeds and accelerations determines the static and dynamic stability margins, used to gage the traversability of the vehicle along the path. The first is the maximum feasible acceleration at zero speed, whereas the second is the maximum feasible speed. Both stability margins are demonstrated for a planar vehicle moving on a sinusoidal path.**

I. Introduction

Stability during motion on rough terrain is essential for autonomous vehicles in space as well as in terrestrial military applications. It is commonly measured by stability margins that take into account various geometric and physical attributes of the vehicle and terrain.

Several vehicle stability margins were previously proposed [6], [10], [14], [15]. These stability margins, however, either do not consider vehicle dynamics or do not consider friction constraints, and none consider terrain surface characteristics. These stability margins are hence not suitable to evaluate vehicle stability during high speed motion on rough terrain. Terrain characteristics were recently considered in the context of planetary exploration [7], however this body of work focuses on simulating the motion of the rover on rough terrain and not on motion planning.

A different approach [17] that accounts for vehicle dynamics offers a *d*ynamic stability margin that consists of the maximum allowable speed under which the vehicle remains stable along its path. It was first derived for a suspended point mass model, and then extended to a planar rigid body [18] and to a Rocker Bogie vehicle [13]. Because of the indeterminate nature of the vehicle system with respect to the ground forces (3 equations and 4 unknowns), these stability margins were computed numerically, which is time consuming. The pseudoinverse method proposed in [9], [18], [13], is deterministic and therefore more efficient, but was shown to provide a too conservative stability margin [18] [13].

This work was performed at the Leo Paslin Robotics Laboratory. It was partly supported by grant 01-99-08430 of the Israeli Space Agency through the Ministry of Science Culture and Sports of Israel.

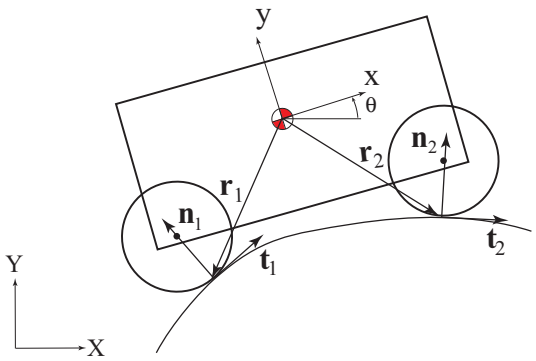

Fig. 1. A planar vehicle model

In this paper, we propose an efficient method to compute the dynamic stability margins of a planar rigid body vehicle. To this end, we wish to determine the feasible range of speed and acceleration along the path that does not violate the vehicle's contact and ground force constraints. This is similar to the classical problem in grasping, where given a rigid body with multiple contact points, one determines the range of net forces that may act upon the object and its accelerations without violating its contact and friction constraints. The two are similar since the net force acting on the object is related to the tangential speed and acceleration of the object's center of mass. The force constraints are computed using a simple terramechanics model that accounts for terrain surface properties. The method is developed for a longitudinal planar vehicle with two wheels.

II. Kinematics

The vehicle is modeled as the planar two-wheel all-wheel drive vehicle shown in Figure 1. For simplicity, we assume that ground forces are applied on the massless wheels of radius r at the tangency points between the wheels and the terrain surface. The position vectors from the c.g. to the back and front contact points, $\mathbf{r}_1$ and $\mathbf{r}_2$, respectively, are expressed in the vehicle's $x-y$ frame shown in Figure 1. The vehicle's orientation θ is measured relative to the inertial frame $X-Y$.

The orientation of the vehicle at any point is computed by modeling the vehicle and its contact points as a closed

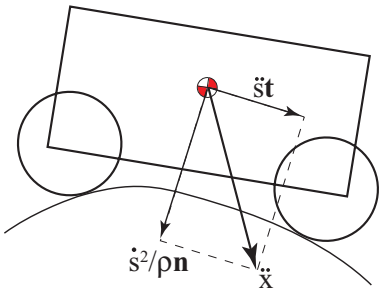

Fig. 2. The acceleration of the center of mass

kinematic chain. The terrain profile is assumed known, so for a given back wheel contact point $\mathbf{x}_1$, we can compute the contact point $\mathbf{x}_2$ of the front wheel. Denoting d as the distance between the two wheel axles and r as the wheel radius, $\mathbf{x}_2$ is found numerically by solving:

$$\| - r\mathbf{n}_1 + \mathbf{x}_2 - \mathbf{x}_1 + r\mathbf{n}_2 \| = d \tag{1}$$

where $\| - \|$ denotes the Euclidean norm. Once $\mathbf{x}_2$ is known, the vehicle's center of mass $\mathbf{x}$, and orientation θ are easily found. The path constraint leaves the vehicle only one degree of freedom in the plane, which can be represented by the arc length, s, along the path followed by the center of mass. The vehicle's linear and angular acceleration are thus expressed in terms of the speed $\dot{s}$ and acceleration $\ddot{s}$ along the path.

The vehicle acceleration $\ddot{\mathbf{x}}$ is decomposed into its tangent and normal components to the path, $\ddot{s}\mathbf{t}$ and $\dot{s}^2/\rho\mathbf{n}$, as shown in Figure 2, where $\mathbf{n}$ points toward the instantaneous center of curvature, and ρ is the radius of curvature. Substituting κ for $(1/\rho)\mathbf{n}$, this transformation to path coordinates is expressed in matrix form:

$$\ddot{\mathbf{x}} = \begin{bmatrix} t_x & \kappa_x \\ t_y & \kappa_y \end{bmatrix} \begin{bmatrix} \ddot{s} \\ \dot{s}^2 \end{bmatrix} = K(s) \begin{bmatrix} \ddot{s} \\ \dot{s}^2 \end{bmatrix} \tag{2}$$

The angular acceleration may be similarly expressed as:

$$\ddot{\theta} = \theta_s \ddot{s} + \theta_{ss} \dot{s}^2 \tag{3}$$

where θ_s and θ_{ss} are the 1^{st} and 2^{nd} derivatives of θ with respect to s.

III. The Ground Forces

The forces developed between the wheel and ground when moving on a horizontal surface are shown in Figure 3. The vehicle applies the normal load W (static and dynamic), the driving torque T, and the reaction force F. The ground in turn applies the normal force F_n and the tangent force F_t that are the resultants of the normal stress σ and shear stress τ (not shown), respectively, developed along the wheel circumference that is in contact with ground [3]. The normal force F_n is normal to the wheel, and its line of action passes through the wheel center. The tangent force F_t is tangent to the wheel and normal to F_n.

Since the surface shown in Figure 3 is horizontal, it is convenient to project the ground forces on the horizontal and vertical axes. The horizontal component of the tangent force is *GT* (Gross Traction), whereas the horizontal component of the normal force is *MR* (Motion Resistance). Clearly, *GT* acts in the direction of motion (forward), whereas *MR* acts in the opposite direction, and thus impedes forward motion. The net traction, *NT*, is the difference between the two:

$$NT = GT - MR. \tag{4}$$

During braking, F_t points in the opposite direction, whereas F_n remains the same. Thus, *MR* decreases the traction force but increases the net braking force, *NB*.

It would be possible to compute the wheel-ground forces if the normal stress σ and shear τ distributions were known. However, σ and τ are difficult to measure, and hence the ground forces can be approximated using any of the existing wheel/ground interaction models. These models can be divided into three main groups: analytical, empirical, and semi-empirical. The analytical models are based on constitutive laws that describe the soil and wheel properties. They employ numerical methods, such as the finite difference methods (FDM) [8], the finite element method (FEM) [11], and the discrete element method (DEM) [2].

The empirical methods [4] are based on a single soil parameter, the cone index (CI), which is simple to measure in situ. The semi-empirical methods, such as Bekker's prediction approach [3], are based on assumptions regarding the interface between the soil and the wheel. The soil parameters are determined by "bevameter" tests [19], which are much harder to obtain than the CI parameter.

Despite the simplicity of the empirical models, they are quite effective in predicting mobility. For this reason, ASAE (the American Society of Agricultural Engineering) has adopted Brixius' empirical model [4] for predicting mobility performance [1]. Recently, predictions obtained by Brixius' model were shown to agree with experimental results and discrete element simulations in the relevant slip rates [2]. There is therefore no practical reason to use other than the simple empirical models.

The Brixius empirical model accounts for soil characteristics using the *cone index CI*. It is determined by pushing a cone into the ground. The depth of penetration of this cone determines the cone index. An average of several cone index values obtained at a test site often yields a representative measure of soil strength [16]. The soil and wheel parameters are combined into the non-dimensional mobility number, B_n, which for a rigid wheel (zero tire deflection) is given by:

$$B_n = \frac{(CI)bd}{W(1+3\frac{b}{d})} \tag{5}$$

where b is the wheel width, and d the wheel diameter.

During motion, the wheel slips relative to the ground surface. The slip is measured by the slip ratio *sr*, defined as:

$$sr = 1 - \frac{V_x}{r\omega}, V_x < r\omega \tag{6}$$

$$sr = 1 - \frac{r\omega}{V_x}, V_x > r\omega \tag{7}$$

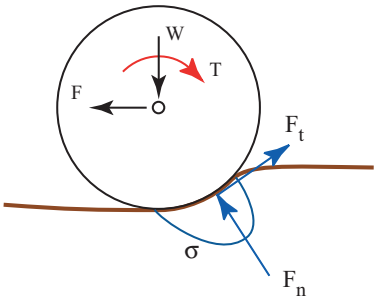

Fig. 3. Forces acting on the wheel

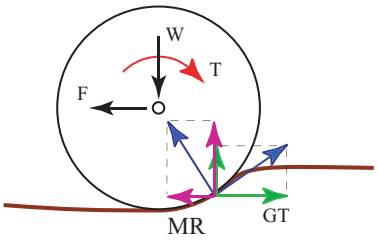

Fig. 4. The horizontal ground forces

where V_x is the velocity of the wheel in the direction of travel, ω is the angular velocity of the wheel, and r is the wheel radius.

The ground forces parallel to the ground surface are predicted using the Brixius empirical model for a given mobility number B_n and slip ratio sr:

$$GT = W0.88(1-e^{-0.1B_n})(1-e^{-7.5sr})+0.04,\ sr>0 \quad (8)$$
$$GT = -W0.88(1-e^{-0.1B_n})(1-e^{7.5sr})+0.04,\ sr<0 \quad (9)$$

$$MR = W(\frac{1}{B_n}+0.04+\frac{0.5sr}{\sqrt{B_n}}),\ sr>0 \quad (10)$$
$$MR = W(\frac{1}{B_n}+0.04-\frac{0.5sr}{\sqrt{B_n}}),\ sr<0. \quad (11)$$

The net traction force NT is thus:

$$NT = W0.88(1-e^{-0.1B_n})(1-e^{-7.5sr})-(\frac{1}{B_n}+\frac{0.5sr}{\sqrt{B_n}}). \quad (12)$$

and the net braking force NB:

$$NB = -W0.88(1-e^{-0.1B_n})(1-e^{7.5sr})-(\frac{1}{B_n}-\frac{0.5sr}{\sqrt{B_n}}). \quad (13)$$

It is convenient to consider the non-dimensional coefficient of the net traction and net braking forces, μ_{NT} and μ_{NB}, respectively:

$$\mu_{NT} = 0.88(1-e^{-0.1B_n})(1-e^{-7.5sr})-(\frac{1}{B_n}+\frac{0.5sr}{\sqrt{B_n}}) \quad (14)$$
$$\mu_{NB} = -0.88(1-e^{-0.1B_n})(1-e^{7.5sr})-(\frac{1}{B_n}-\frac{0.5sr}{\sqrt{B_n}}) \quad (15)$$

These coefficients can be viewed as slip dependent coefficients of friction. Figures 5 and 6 show plots of traction and braking ratios for $B_n = 55$, corresponding to a firm ground, and $B_n = 20$, corresponding to sandy soil [1]. The traction

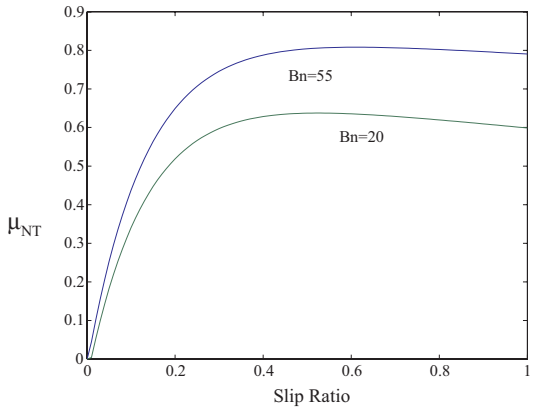

Fig. 5. Coefficient of net traction μ_{NT} as a function of slip ratio sr.

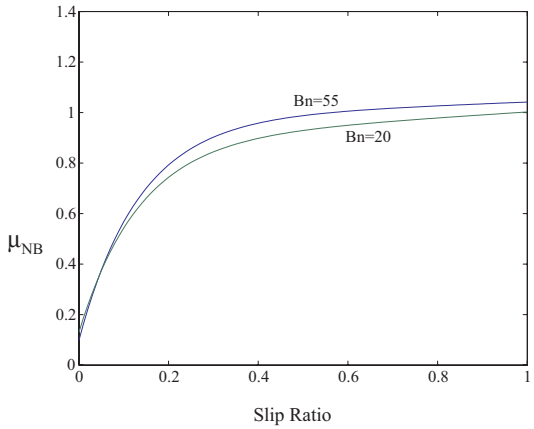

Fig. 6. Coefficient of net braking μ_{NB} as a function of slip ratio sr.

ratio declines beyond some peak value, whereas the braking ratio keeps increasing with slip. Practically, it is desirable to stay at slip ratios below 0.3 to prevent soil failure that may cause loss of vehicle control.

The ground forces were presented for a horizontal surface. Their modification for an inclined plane is trivial and will be omitted in this paper. During forward motion, the ground forces act at some point ahead of the wheel center. For simplicity, we will move this point back to the tangency point between the wheel and the ground surface.

Limiting the slip ratio to 0.3 imposes constraints on the ground forces:

$$NT_1 \le \mu_{NT}(sr=0.3)N_1 \quad (16)$$
$$NT_1 \ge -\mu_{NB}(sr=0.3)N_1 \quad (17)$$
$$NT_2 \le \mu_{NT}(sr=0.3)N_2 \quad (18)$$
$$NT_2 \ge -\mu_{NB}(sr=0.3)N_2 \quad (19)$$

where N is the reaction force normal to the ground surface.

IV. Vehicle Dynamics

The equations of motion for the vehicle are:

$$\mathbf{f_1}+\mathbf{f_2}+m\mathbf{g} = m\ddot{\mathbf{x}} \quad (20)$$
$$\mathbf{r_1}\times\mathbf{f_1}+\mathbf{r_2}\times\mathbf{f_2} = I\ddot{\theta} \quad (21)$$

where $\mathbf{f}_i$ represents the ground force acting on each wheel:

$$\mathbf{f}_i = NT_i\mathbf{n}_i + N_i\mathbf{t}_i, i = 1,2 \tag{22}$$

Substituting (2) into (20) and (3) into (21) yields the equations of motion in terms of the speed and acceleration along the path:

$$\mathbf{f}_1 + \mathbf{f}_2 + m\mathbf{g} = mK(s)\begin{bmatrix} \ddot{s} \\ \dot{s}^2 \end{bmatrix} \tag{23}$$

$$\mathbf{r_1} \times \mathbf{f_1} + \mathbf{r_2} \times \mathbf{f_2} = I(\theta_s\ddot{s} + \theta_{ss}\dot{s}^2) \tag{24}$$

Equations (23) and (24) relate any applied forces $\mathbf{f_1}$ and $\mathbf{f_2}$ to the corresponding $\dot{s}$ and $\ddot{s}$. The constraints on $\mathbf{f_1}$ and $\mathbf{f_2}$ thus map to constraints on $\dot{s}$ and $\ddot{s}$, which determine the static and dynamic stability margins derived next.

Note that (20) and (21) are coupled since the vehicle is traversing a given terrain profile and thus the angular acceleration is determined from its linear acceleration. The moment equation (21) hence imposes a constraint on the ground forces. This constraint can be derived as an equality constraint by substituting (2) into (3) to express $\ddot{\theta}$ in terms of $\ddot{\mathbf{x}}$, then replacing $\ddot{\mathbf{x}}$ with the left hand side of (20) to yield:

$$\begin{aligned} \mathbf{r_1} \times \mathbf{f_1} + \mathbf{r_2} \times \mathbf{f_2} &= I\begin{bmatrix} \theta_s & \theta_{ss} \end{bmatrix} K^{-1}\left(\frac{\mathbf{f}_w}{m} + \mathbf{g}\right) \quad (25) \\ &= \begin{bmatrix} v_1 & v_2 \end{bmatrix} \cdot \left(\frac{\mathbf{f}_w}{m} + \mathbf{g}\right) \end{aligned}$$

where v_1 and v_2 are the two scalar components of the vector $\{I\begin{bmatrix} \theta_s & \theta_{ss} \end{bmatrix} K^{-1}\}$, and the sum of the ground forces is

$$\mathbf{f}_w = \mathbf{f}_1 + \mathbf{f}_2 \tag{26}$$

Rearranging (25) yields:

$$\mathbf{f}_1 + \mathbf{f}_2 + m\mathbf{g} = m\ddot{\mathbf{x}} \tag{27}$$

$$\bar{\mathbf{r}}_1 \times \mathbf{f_1} + \bar{\mathbf{r}}_2 \times \mathbf{f_2} + \bar{\mathbf{r}}_3 \times m\mathbf{g} = 0 \tag{28}$$

where

$$\bar{\mathbf{r}}_1 = \mathbf{r}_1 + \bar{\mathbf{r}}_3 \tag{29}$$

$$\bar{\mathbf{r}}_2 = \mathbf{r}_2 + \bar{\mathbf{r}}_3 \tag{30}$$

$$\bar{\mathbf{r}}_3 = \begin{bmatrix} -v_2 & v_1 \end{bmatrix} \tag{31}$$

Equation (28), in comparison to (21), represents the moment equation of an equivalent system that has a zero moment of inertia, and a virtual point that we call ZMP (zero moment point) where the moments of all external forces applied on the system, including the gravity force, are zero. Note that the moments is, generally, not zero around the center of mass because of the angular acceleration of the rigid body along the path. Thus, satisfying a zero moment around the ZMP is a necessary condition on the ground forces so that the vehicle tracks the desired path.

The ZMP is located at $-\bar{\mathbf{r}}_3$ from the center of mass, as is shown in Figure 7. Note that $\bar{\mathbf{r}}_3$ reflects the body's inertial parameters as well as the path curvature. The forces acting upon the equivalent system, however, have not changed, and so (20) still holds. Our goal now is to find the set of admissible accelerations that are produced by the ground forces that satisfy the friction constraints and the equality constraint (28). The set of admissible accelerations would yield the desired dynamic stability margins.

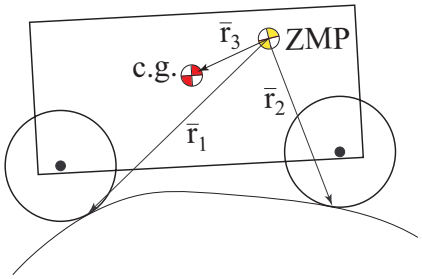

Fig. 7. The Zero Moment Point.

V. Computing the Set of Admissible Accelerations

The set of admissible accelerations is a convex polygon in the plane of $\mathbf{f}_1$ and $\mathbf{f}_2$ since both are constrained by a set of linear inequality and equality constraints [5]. This polygon is the intersection of half planes, each satisfying two of the four inequality constraints ((16)- (19)) and the equations of motion ((27)) ((28)). The boundary of each half plane is determined by considering the equality part of the respective inequality constraints.

There are four independent ground forces acting on the vehicle: the net traction and normal forces on both wheels. Applying the moment constraint (28) reduces the set of feasible forces to a three dimensional manifold in $\mathbb{R}^4$. Adding two frictional constraints reduces this further to a line in $\mathbb{R}^4$.

We derive the equation of this line by first writing the force equation (23) in matrix form:

$$A\begin{bmatrix} NT_1 \\ N_1 \\ NT_2 \\ N_2 \end{bmatrix} = mK(s)\begin{bmatrix} \ddot{s} \\ \dot{s}^2 \end{bmatrix} \tag{32}$$

where

$$A = \begin{bmatrix} \mathbf{t}_1 & \mathbf{n}_1 & \mathbf{t}_2 & \mathbf{n}_2 \end{bmatrix}$$

We then combine the moment equation (28) with two of the four traction constraints (16 19) in matrix form to obtain

$$B\mathbf{f} = \mathbf{z} \tag{33}$$

where

$$B = \begin{bmatrix} 1 & -\mu & 0 & 0 \\ 0 & 0 & 1 & -\mu \\ \mathbf{r}_1 \times \mathbf{t}_1 & \mathbf{r}_1 \times \mathbf{n}_1 & \mathbf{r}_2 \times \mathbf{t}_2 & \mathbf{r}_2 \times \mathbf{n}_2 \end{bmatrix}$$

$$\mathbf{f} = \begin{bmatrix} NT_1 \\ N_1 \\ NT_2 \\ N_2 \end{bmatrix}$$

and

$$\mathbf{z} = \begin{bmatrix} 0 \\ 0 \\ -\bar{\mathbf{r}}_3 \times m\mathbf{g} \end{bmatrix}$$

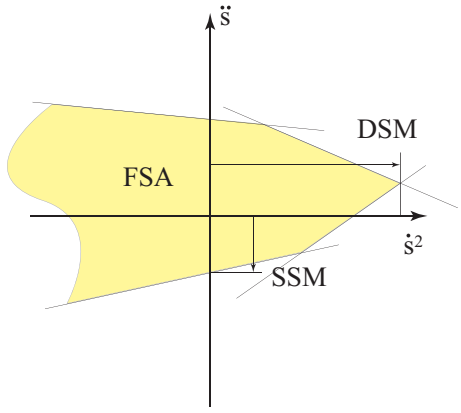

Fig. 8. The Feasible range of Speed and Acceleration (FSA).

The set of forces satisfying (33) forms a line in $\mathbb{R}^4$ as stated earlier. To calculate the parametric equation of this line, we partition $\mathbf{f}$ into its dependent components, NT_1, N_1, NT_2, and its independent parameter N_2. We must likewise partition B into the first three columns that multiply the dependent variables and the fourth column that multiplies N_2, such that

$$B = \begin{bmatrix} & B_1 & & |\mathbf{b}_2| \end{bmatrix} \tag{34}$$

The matrix B_1 is square and generally invertible (depending on the choice of constraints), which enables us to solve for the first three forces:

$$\begin{bmatrix} NT_1 \\ N_1 \\ NT_2 \\ \hline N_2 \end{bmatrix} = \begin{bmatrix} B_1^{-1}(\mathbf{z} - \mathbf{b}_2 N_2) \\ \hline N_2 \end{bmatrix} \tag{35}$$

Substituting (35) into (32) yields:

$$A \begin{bmatrix} B_1^{-1}(\mathbf{z} - \mathbf{b}_2 N_2) \\ \hline N_2 \end{bmatrix} = mK(s) \begin{bmatrix} \ddot{s} \\ \dot{s}^2 \end{bmatrix} \tag{36}$$

Equation (36) represents two equations in N_2. Eliminating N_2 produces one equation in $\ddot{s}$ and $\dot{s}^2$ of the form

$$a\ddot{s} + b\dot{s}^2 + c = 0. \tag{37}$$

Equation (37) represents a line in the $\ddot{s} - \dot{s}^2$ plane due to one pair of the four traction constraints (16 - 19). This line represents the equality part of the two constraints. Considering the inequality constraints would produce a half plain in the $\ddot{s} - \dot{s}^2$ space. Repeating this procedure for the six different pairs of constraints produces at most four half planes [12], the intersection of which forms the set of feasible speeds and accelerations, FSA shown in Figure 8.

VI. Stability Margins

The set FSA shown in Figure 8 consists of all speeds and accelerations that are attainable by the feasible ground forces. Any given pair of speed (squared) and acceleration that lies outside of the FSA region is obviously unattainable.

The dynamic stability margin, DSM, was defined in [18] as the maximum feasible speed, whereas the static stability margin, SSM, as the minimum feasible acceleration range at zero speed. The stability margins are indicated in Figure 8 on the boundaries of FSA:

$$DSM(s) = \begin{cases} max(\dot{s}), \dot{s}^2 \in FSA & \text{if } max(\dot{s}) \geq 0 \\ 0 & \text{otherwise} \end{cases} \tag{38}$$

$$SSM(s) = \begin{cases} min(|\ddot{s}_{min}|, |\ddot{s}_{max}|)_{\dot{s}=0} & \text{if } \ddot{s}_{max} > 0,\ \ddot{s}_{min} < 0 \\ = 0 & \text{otherwise} \end{cases} \tag{39}$$

The SSM and DSM are important indicators of the stability of a vehicle traversing a preset trajectory. For example, a vehicle on a steep incline will have a low SSM, indicating that slippage is likely to occur if the vehicle accelerates too rapidly. A vehicle on a convex surface will have a low DSM, which indicates that a sufficiently high velocity will result in the vehicle losing contact with the surface. Both stability margins reflect the vehicle parameters, and terrain topography and traction. The asymmetric soil properties for acceleration and braking affect the stability margins through the parameters of the lines produced in (37) for every pair of traction constraints (16 - 19).

VII. Examples

The stability margins developed in this paper are demonstrated for a planar vehicle traversing the sinusoidal track shown in Figure 9. The static and dynamic stability margins for the entire path are shown in Figure 10. Generally, the

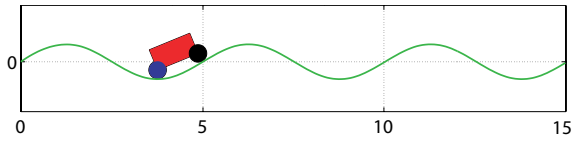

Fig. 9. A vehicle on a sinusoidal track.

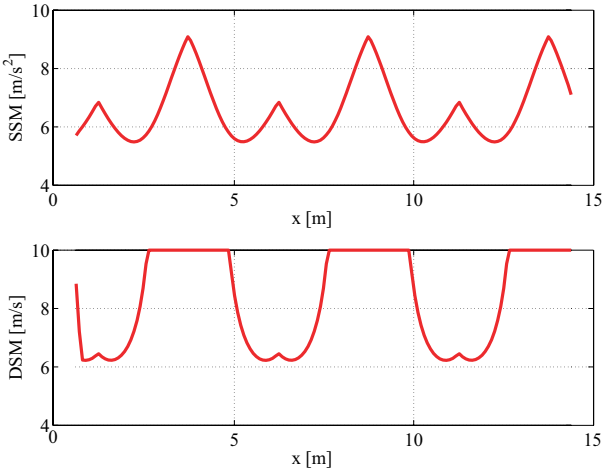

Fig. 10. The SSM and DSM for a vehicle traversing a sinusoidal track.

DSM is higher at the bottom of the hill, due to the concavity of the surface, where higher speeds elicit greater traction. On

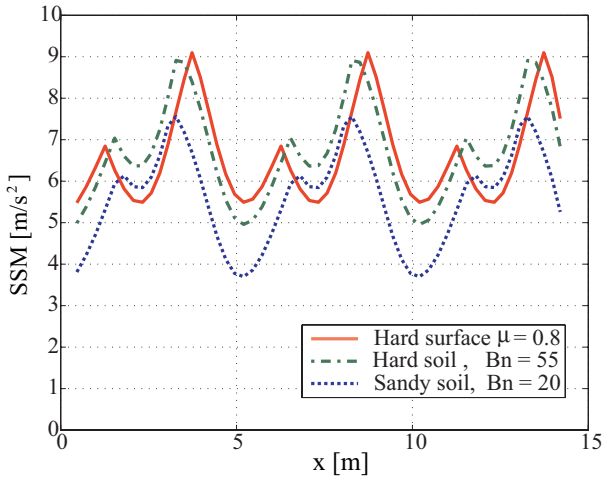

Fig. 11. The SSM for a vehicle traversing a sinusoidal path on hard surface, hard soil, and sandy soil.

the other hand, the DSM is lower at the top of the hill, where the ground forces are reduced due to the radial acceleration. The SSM is low along the inclines of the hill, where the acceleration is reduced to the gravity force. It is higher at the top and bottom of the hills where the vehicle is horizontal and its acceleration not affected by the gravity force.

Computing the stability margins for the same vehicle on hard and sandy soil resulted in almost no change for the DSM, implying that the soft soil does not explicitly limit the vehicle speeds. This result makes sense since the traction and braking coefficients are not affected by speed. The vehicle speed is limited by its tendencies to tipover, fly into the air, or slide, which are dictated by the terrain profile and vehicle parameters. An interesting difference between hard and soft soil was demonstrated for the SSM. Figure 11 shows the SSM for three different grounds: paved, hard soil ($B_n = 55$), and sandy soil ($B_n = 20$). The traction and braking coefficients were computed at slip ratio $sr = 0.3$. At $sr = 0.3$, $\mu_{NT}(B_n = 55) = 0.74$, $\mu_{NT}(B_n = 20) = 0.60$, $\mu_{NB}(B_n = 55) = 0.90$, $\mu_{NB}(B_n = 20) = 0.84$.

The SSM for the hard surface is symmetric due to the symmetric coefficient of friction, whereas in the case of unpaved surface, the SSM is lower on the uphill and higher on the downhill, due to the asymmetric contribution of the motion resistance force (impeding traction and enhancing braking). The softer the soil the greater the difference. This suggests that soil characteristics affect static stability and acceleration, and thus would result in slower motion on uphill segments than on paved surfaces.

VIII. Conclusions

This paper presented a simple procedure to determine the dynamic stability of a planar vehicle traveling on rough terrain. The ground forces are computed using a simple terramechanics model. This model determines the traction and braking force constraints, which together with the vehicle's equations of motion are mapped into the range of admissible speeds and tangential accelerations. The boundaries of this range determine the static and dynamic stability margins. The first is the maximum acceleration at zero speed, whereas the latter is the maximum feasible speed that does not violate ground force constraints. The dynamic stability margins have been shown to be an effective metric for computing optimal trajectories over general terrain [17]. Soil characteristics was shown to affect the static stability margin, but not the dynamic stability margin. The proposed rapid computation enables autonomous vehicles to quickly and safely traverse rough terrain, an essential feature for future robotic missions in urban and off-road environments.

References

[1] ASAE Standards. D497.4. Agricultural Machinery Management Data. St. Joseph, MI, USA, 2003.

[2] Asaf, Z., I. Shmulevich and D. Rubinstein, "Predicting soil-rigid wheel performance using discrete element method", Transactions of the ASABE 49(3), 2006: 607-616.

[3] Bekker, M. G.: *Theory of Land Locomotion*. Ann Arbor, Mich.: University of Michigan Press, 1956.

[4] Brixius, W. W, 1987. Traction prediction equations for bias ply tires. ASAE paper no. 87-1622, ASAE, St. Joseph, MI 49085.

[5] M. de Berg, M. van Kreveld. M. Overmars, O. Schwarzkopf, *Computational Geometry*, Springer, 2000.

[6] E. Garcia, J. Estremera, P.G. de Santos, "A Comparative Study of Stability Margins For Walking Machine",*Robotica* Vol. 30, pp. 595-606, 2002.

[7] G. Ishigami, A. Miwa, K,. Yoshida, "Steering Trajectory Analysis of Planetary Exploration Rovers Based on All-Wheel Dynamics Model," Proc. ISAIRAS, Munich, Germany, Sept. 2005.

[8] Karafiath, L. K., and E. A. Nowaizki. 1978. Soil Mechanics for Off Road Vehicle Engineering. Clausthal, Germany: Trans Tech Publications.

[9] C.A. Klein, T.S. Chung, "Force Interaction and Allocation for the Legs of a Walking Vehicle", *IEEE Transactions of Robotics and Automation*, Vol RA-3, No. 6, Dec. 1987.

[10] B. Lin, S. Song, "Dynamic Modeling, Stability, and Energy Efficiency of a Quadrupedal Walking Machine", Proc. IEEE Conf. on Robotics and Automation, Atlanta, Georgia, 1993, pp. 367-373.

[11] Liu, C. H., and J. Y. Wong. 1996. Numerical simulations of tire-soil interaction based on critical state soil mechanics. J. Terramechanics 33(5): 209-221.

[12] M. Mann: "Dynamic Stability of off-road Vehicles", M.S. Thesis, Mechanical Engineering, Technion, in preparation.

[13] M. Mann, Z. Shiller: "Dynamic Stability of a Rocker Bogie Vehicle: Longitudinal Motion", Proc. IEEE Conf. on Robotics and Automation, Barcelona, Spain, April 2005.

[14] R.B. McGhee, A.A. Frank: "On the Stability Properties of Quadruped Creeping Gait", *Mathematical Biosciences*, Vol. 3, No. 2, pp. 331-351, 1968. Legged Vehicle with respect to Maneuverability", PhD Thesis, Ohio State University, 1985.

[15] E. Papadopulos, D. Rey: "The Force-Angle Measure of Tipover Stability Margin for Mobile Manipulators", *Vehicle System Dynamics*, Vol. 33, No. 1, pp. 29-48, 2000.

[16] Schmid, I. C. 1995. Interaction of vehicle and terrain results from 10 years research at IKK. *J. Terramechanics*. Vol. 32(1) 3-26.

[17] Z. Shiller, Y.R. Gwo: "Dynamic Motion Planning of Autonomous Vehicles", *IEEE Transactions on Robotics and Automation*, Vol. 7, No. 2, April 1991.

[18] Z. Shiller, M. Mann: "Dynamic Stability of Off Road Vehicles", Proc. IROS 2004, Sendai, Japan, October 2004, pp. 1849-1853.

[19] Wong, J. Y. 1989. Terramechanics and Off-Road Vehicles. Amsterdam, The Netherlands: Elsevier. Stability Criterion of Integrated Locomotion and Manipulation, *Journal of Robotics and Mechatronics*, Vol. 9, No. 4, pp. 267-274.